Simultaneous measurements of refractive index and temperature based on a no-core fiber coated with Ag and PDMS films

Yuxin Li(李宇昕)[1], Hailiang Chen(陈海良)[1,†], Yingyue Zhang(张赢月)[1], Qiang Chen(陈强)[1], Biao Wu(武彪)[1], Xiaoya Fan(樊晓亚)[1], Yingchao Liu(刘英超)[2], and Mingjian Ma(马明建)[1]

[1] *State Key Laboratory of Metastable Materials Science & Technology and Key Laboratory for Microstructural Material Physics of Hebei Province, School of Science, Yanshan University, Qinhuangdao* 066004, *China*

[2] *College of Artificial Intelligence, North China University of Science and Technology, Tangshan* 063210, *China*

(Received 18 April 2022; revised manuscript received 1 July 2022; accepted manuscript online 5 September 2022)

A compact surface plasmon resonance (SPR) fiber optic sensor, being utilized to simultaneously measure refractive index (RI) and temperature, is proposed and experimentally demonstrated in this paper. One part of a no-core fiber (NCF) was coated with a silver (Ag) film, and the other part was coated with a silver/polydimethylsiloxane (Ag/PDMS) composite film to stimulate the SPR effect. Due to the two heterogeneous films, two dips appeared in the transmission spectrum and were used to achieve the dual-parameter measurements. The experimental results showed that the RI sensitivity reached 2121.43 nm/RIU and 0 nm/RIU, while the temperature sensitivity reached −0.32 nm/°C and −2.21 nm/°C for the two dips, respectively. Based on the obtained transfer matrix, the measurements of RI and temperature could be demodulated. This designed sensor showed the merits of simple structure, easy to implement, and high sensitivity, demonstrating application prospects in dual-parameter monitoring.

Keywords: no-core fiber, surface plasmon resonance, temperature sensor

PACS: 42.81.Qb, 71.45.Gm, 07.07.Df **DOI:** 10.1088/1674-1056/ac8f36

1. Introduction

Optical fiber sensors have many advantages, such as high integration, small size, anti-electromagnetic interference, and remote real-time monitoring. They have shown broad application prospects in food safety, chemical molecular detection, and pharmaceutical analysis.[1–3] Due to their high sensitivity to variation in their surroundings, optical fiber sensors were more attractive for use in humidity, temperature, and refractive index (RI) sensing.[4–6] Surface plasmon resonance (SPR) is a widely used analysis method that can detect changes in the RI of the adsorption layer or the temperature of the external environment with high sensitivity.[7,8] The optical fiber-based SPR sensor has the advantages of simple structure, lower price, multi-channel sensing, and short response time.[9] Compared with the prism-based SPR sensor, it is more suitable for remote sensing applications. Fiber optic SPR sensors have been widely studied and applied in many fields because of their excellent performance and ability to adapt to different environmental requirements.[10,11] SPR-based sensors have relied on the resonance between optical evanescent waves and metal surface plasmon waves (SPW) to make a dip appear in the spectrum.[12] This dip is called the resonance wavelength, which can be modulated by the surrounding mediums. The wavelength interrogation method is usually used to perceive the change in the medium around the optical fiber SPR sensor.

In-depth research has been conducted on fiber sensors, and various sensors for measurement of the RI have been reported in recent years.[13] The measurement of the refractive index had important significance and practical value in the fields of chemistry, physics, and especially bio-sensing.[14–16] However, the detection of the refractive index was usually affected by the ambient temperature. How to better deal with the influence of temperature was a problem faced by the development of refractive index sensors. Christophe *et al.* proposed a refractive index sensor based on tilted-fiber Bragg gratings and surface plasmon resonance. The sensitivity of the sensor was 535 nm/RIU for RI sensing.[17] In 2018, a refractive index sensor based on microfiber coated with gold nanowires was proposed by Zhan *et al.* The sensitivity of the sensor was improved and achieved 5200 nm/RIU.[18] Zhang *et al.* proposed an SPR and multimode interference (MMI)-based optical fiber sensor to measure RI and temperature.[19] The sensitivity of the sensor was 2061.6 nm/RIU for RI detection and 37.9 pm/°C for temperature detection. Different physical principles, such as the SPR principle and the MMI principle, showed different difficulties in the sensor production. By filling a hollow-core fiber with isopropanol, Liu *et al.* designed a dual-parameter measurement scheme.[20] The temperature sensitivity was −42.7 pm/°C from room temperature to 80 °C, while the refractive index sensitivity was 141 nm/RIU for the surrounding liquid. However, it was not easy to fill the optical fiber with the medium. Sun *et al.* proposed a sensor for measuring refractive index and temperature with a structure composed of multimode fiber (MMF) and thin-core fiber fusion

†Corresponding author. E-mail: hlchen@ysu.edu.cn

© 2023 Chinese Physical Society and IOP Publishing Ltd

splicing.[21] The RI sensitivities at interference dip1 and dip2 were −30.290 nm/RIU and −79.335 nm/RIU, respectively. The temperature sensitivities based on interference dip1 and dip2 were 0.065 nm/°C and 0.053 nm/°C, correspondingly. These previously proposed sensors showed the characteristics of dual-parameter measurement. However, the sensitivity of these sensors was not very high.

In this paper, we propose a compact and highly sensitive dual parameter NCF sensor based on SPR, which can measure the RI and ambient temperature. The sensor consists of MMF-NCF-MMF. The NCF is coated with silver film and silver/polydimethylsiloxane composite film using the magnetron sputtering method to excite the SPR. By tracing two different dips in the spectrum, the temperature and RI variations can be measured simultaneously. Compared with previously reported sensors, this proposed sensor exhibits a great improvement in sensitivity in the measurement of RI and temperature. The maximum sensitivities are 8100 nm/RIU for RI detection in the range of 1.333–1.363 and 1.3 nm/°C for temperature detection in the range of 35 °C–60 °C, respectively. Our designed SPR-based sensor can be utilized to monitor the temperature and RI with high precision due to the characteristics of high sensitivity.

2. Experimental setup and operation principles

Since the optical fiber SPR effect possesses the characteristics of a wider spectrum, the wavelength of modulation characteristics develops well.[22] On this basis, a combination of MMF, NCF and MMF is designed, as shown in Fig. 1(a). The core and cladding diameters of the MMF are 62.5 μm and 125 μm, respectively. The cladding diameter of the NCF is 125 μm, and its length is fixed at 2.8 cm. We chose the NCF because of its special core structure. When the optical signal is transmitted from the MMF to the NCF, it is easy to stimulate the SPR effect on the surface of the metal film. The MMF can be used as a carrier for the input and collection of optical signals. When the MMF transmits optical signals, there are multiple modes in the optical fiber. The MMF makes more light enter the surface of the coreless fiber to excite SPR. It can also carry out long-distance and low-loss transmission in the visible light band. Compared with other common plasma materials, Ag can obtain a sharper resonance dip.[23] Therefore, the SPR effect is stimulated by sputtering a Ag film on the surface of the NCF. The sensitive film is wrapped at the part of the NCF coated with Ag film to measure temperature. The exposed NCF coated with Ag film experiences changes in refractive index in a liquid environment.

Figure 1(b) shows the brief procedure of the structure processing method of the SPR-based optical fiber sensor. Firstly, the surface of the NCF is cleaned with ethanol. Secondly, the cleaned NCF is placed in the magnetron sputtering equipment for metal coating. The sample holder in the sample chamber is constantly rotating to ensure that the Ag film is uniform. The voltage and current are fixed at 1000 mV and 200 mA, respectively. The sputtering time is 210 s. The Ag-coated NCF is taken out of the magnetron sputtering equipment to splice it in the middle of the MMF using a fusion splicer. Finally, the part of the Ag-coated NCF that has been fused is coated with a temperature-sensitive material. The temperature-sensitive material here is PDMS. The PDMS used in the experiment is Sylgard-184 (Dow Corning), which includes polymer (Sylgard-184-A) and curing agent (Sylgard-184-B). The main component of the polymer is a prepolymer and a small amount of platinum catalyst, and the curing agent is a prepolymer with vinyl side chains and a cross-linking agent. The specific operation is as follows: the polymer and curing agent are mixed at a mass ratio of 10:1, stirred evenly, and then allowed to stand still until there are no bubbles to obtain a uniform colloidal mixture. The colloidal mixture is then evenly applied to the sensing area of the temperature sensor. The PDMS is coated on the optical fiber and heated to accelerate its curing. As shown in Fig. 2(a), the fiber optic sensor based on SPR is connected between broadband light sources (AvaLight-Hal-(S)-mini, 360 nm–2500 nm), and the spectrometer (Ocean Optics Inc., USB 4000, 350 nm–1100 nm) through several MMFs. Figure 2(b) is a detailed view of the NCF coated with Ag and Ag/PDMS film on the temperature-control box. Then, the spectrometer is connected to the computer. The wavelength range of the broadband light source is 360 nm–2500 nm, and the spectral range of the spectrometer is 350 nm–1100 nm. The refractive index is modified by adding an analyte to the surface of the Ag-plated-PDMS coreless fiber, and the outside temperature is controlled by a temperature-control box. The transmitted optical signal is observed and recorded by a computer connected to the spectrometer.

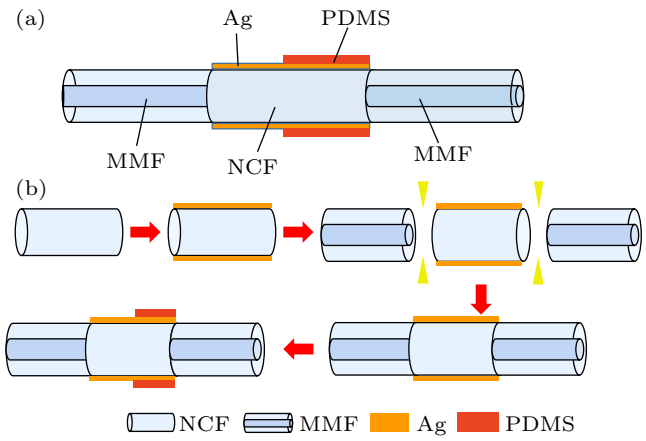


Fig. 1. (a) A schematic diagram of the proposed SPR sensor structure, and (b) the brief process of the structure processing procedure.

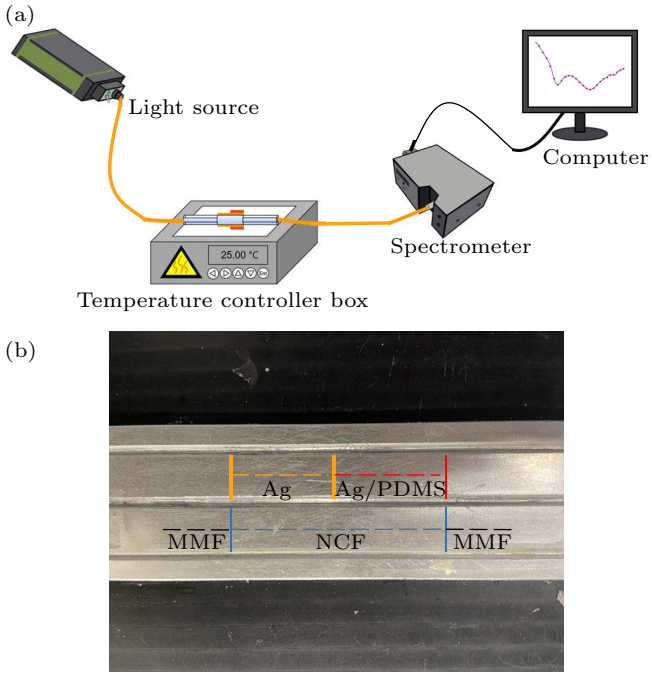


Fig. 2. (a) The experimental setup of the fiber optic SPR sensor, and (b) the NCF sensor during the experiment.

The fiber optic SPR sensor is based on the SPR principle,[22] which usually occurs at the interface between the metal and dielectric. When two electromagnetic waves propagate in the same direction at the same wave vector and frequency they will resonate with each other. The evanescent wave generated by total reflection can exist at the metal-medium interface through the metal layer, when the thickness of the metal layer is less than the effective depth of the evanescent wave. The wave vector of the evanescent wave in the x-direction is expressed as[23]

$$k_x = \frac{\omega}{c}\sqrt{\varepsilon_0}\sin\theta, \tag{1}$$

where ε_0, θ, and ω are the dielectric constant of the fiber core, the angle of the incidence light, and the frequency of the incident light, respectively. According to the SPR radiation-free transient electromagnetic field and the corresponding boundary conditions of Maxwell's equations, we can obtain[24]

$$\frac{\varepsilon_1}{\sqrt{k_{\rm sp}^2 - \varepsilon_1(\omega/c)^2}} = \frac{\varepsilon_2}{\sqrt{k^2 - \varepsilon_2(\omega/c)^2}}. \tag{2}$$

Here, $k_{\rm sp}$ is a wave vector of the surface plasma wave. The propagation constant of the surface plasma wave propagating at the interface between the dielectric and metal is given by the following expression:[25]

$$k_{\rm sp} = \frac{\omega}{c}\sqrt{\frac{\varepsilon_1\varepsilon_2}{(\varepsilon 1 + \varepsilon 2)}}, \tag{3}$$

where ε_1 is the dielectric constant of the metal film, and ε_2 is the dielectric constant of the environmental medium around the metal film. Therefore, the real part of the surface plasmon wave vector and the evanescent wave vector has the same x-direction component to explain the excitation conditions of SPR. When $k_x = \text{real}\,(k_{\rm sp})$, SPR occurs.

In the SPR-based dual-sided polished photonic crystal fiber (PCF) sensor, it is assumed that the resonance wavelength shifts corresponding to the two resonance dips are $\Delta\lambda_{\rm I}$ and $\Delta\lambda_{\rm II}$.[26] The two resonance dips change linearly with temperature and the refractive index. The influence of temperature and the refractive index on the resonance wavelength can be defined as

$$\begin{bmatrix}\Delta\lambda_{\rm I}\\ \Delta\lambda_{\rm II}\end{bmatrix} = \begin{bmatrix}K_{T\rm I} & K_{n\rm I}\\ K_{T\rm II} & K_{n\rm II}\end{bmatrix}\cdot\begin{bmatrix}\Delta T\\ \Delta n\end{bmatrix} = K\begin{bmatrix}\Delta T\\ \Delta n\end{bmatrix}, \tag{4}$$

where ΔT and Δn are variations in temperature and refractive index, $K_{T\rm I}$ and $K_{T\rm II}$ are the temperature fitting coefficients, while $K_{n\rm I}$ and $K_{n\rm II}$ are the refractive index fitting coefficients.

2.1. Results and discussion

During the experiment, we use the light intensity when the surrounding medium is air as the reference spectrum, and evaluate the sensing performance by analyzing the changes in the transmission spectrum. This allows us to obtain the wavelength range of the resonant dip of the NCF coated with Ag film and the influence of temperature and refractive index changes on it. The first experiment was the refractive index and temperature measurement experiment of Ag-plated NCF. The NCF is placed in the magnetron sputtering equipment for Ag coating. The voltage and current are fixed at 1000 mV and 200 mA, respectively. The sputtering time is 210 s. The Ag-coated NCF is taken out of the magnetron sputtering equipment to splice it in the middle of the MMF using a fusion splicer. The length of the NCF is 2.8 cm. When measuring the refractive index, we adjust the temperature of the temperature-control box at 25 °C. We drop the liquid analyte on the surface of the NCF coated with Ag to measure the refractive index. The refractive index of the solution to be tested ranges from 1.333 to 1.375. Figure 3(a) shows the transmission spectra obtained under different refractive indexes. It can be seen that as the RI of the liquid increases, the transmission spectrum shows a red shift. Figure 3(b) shows the fit of the refractive index to the wavelength of its resonance dips. The total displacement of the resonance wavelength reaches 103 nm when the liquid RI changes from 1.333 to 1.375. The linear fitting expression of the resonant wavelength of the RI vs. the RI is $y = 2200.18x - 2415.43$, where y and x represent the resonance wavelength and RI, respectively. The sensitivity of the RI and the linearity R^2 are 2200.18 nm/RIU and 0.98527, respectively.

Then, the temperature sensing test was performed on the NCF coated with Ag film. We dropped deionized water with a

refractive index of 1.333 on the surface of the Ag-coated NCF and kept it unchanged. The temperature was changed by adjusting the temperature-control box. The temperature-control box can tune the temperature from 25 °C to 65 °C. Figure 4 shows the transmission spectrum at different outside temperatures. It can be seen that as the outside temperature increases, the transmission spectrum shows a weak blue shift.

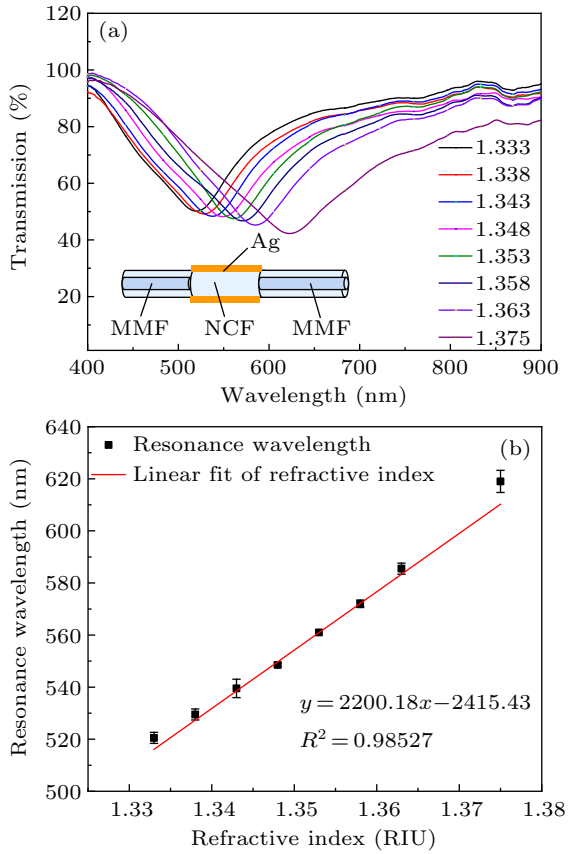


Fig. 3. (a) Transmission spectra at different RI, and (b) resonance wavelength variation with RI.

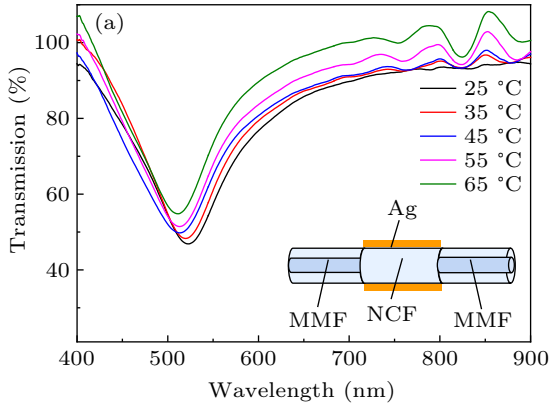


Fig. 4. Transmission spectra at different temperatures.

From the above conducted experiment, we can conclude that the refractive index has a greater impact on the sensor structure of the NCF coated with Ag film. The resonance dip appears near the 500–600 nm wavelength range. When the temperature changes, the refractive index of the deionized water dropped on the surface of the Ag-coated NCF will change with the increases in temperature. The change in the refractive index of an aqueous solution with temperature follows the formula[26] $n_{\mathrm{wat}} = -1.35 \times 10^{-4} T + 1.3359$. Therefore, when the temperature changes and there is deionized water on the sensing area, the resonance dip of the sensor with this structure will only have a slight deviation. Moreover, the sensor presented reliable results in terms of repeatability according to the random uncertainties contained in the error bars of Fig. 3(b); the maximum standard deviation is 4.24. In the near infrared band, the standard deviation of the resulting spectral variation can be approximated by

$$\tau = (\mathrm{FWHM})/(4.5 \times (\mathrm{SNR})^{0.25}), \tag{5}$$

where SNR is 60 dB in such a spectrum with good quality, as in Ref. [27]. The maximum FWHM in the experiments is 180 nm. Therefore, the standard deviation of the spectral variation calculated by Eq. (5) is 1.249.

To obtain the wavelength range of the resonant valley of the NCF coated with Ag/PDMS film and the influence of temperature and refractive index changes on it, we conducted the second experiment: this involved plating a Ag/PDMS film on NCF to measure temperature and the refractive index. The NCF is placed in the magnetron sputtering equipment for plating with Ag film. The voltage, current, and sputtering time are the same as in the above experiment. The Ag-plated NCF is spliced to the middle of the MMF with a fusion splicer. The Ag-coated NCF that has been fused is coated with PDMS. The uniform colloidal mixture is coated on the Ag-plated NCF and is heated to accelerate its curing. The length of the NCF is 2.8 cm. During the temperature sensing test, we dropped deionized water with a refractive index of 1.333 on the surface of the Ag/PDMS-coated NCF. The temperature is adjusted by the control box from 20 °C to 70 °C. The transmission spectrum at different outside temperatures is shown in Fig. 5(a). It can be seen that as the outside temperature increases, the transmission spectrum has a weak blue shift. Figure 5(b) shows the fitting of temperature and its resonant dip wavelength. When the temperature changes from 20 °C to 70 °C, the total shift of the resonance wavelength is 96 nm. The linear fitting expression of the resonant wavelength of the temperature vs. the temperature is $y = -1.96x + 775.10$, where y and x represent the resonance wavelength and temperature, respectively. The sensitivity of the RI and the linearity R^2 are −1.96 nm/°C and 0.99624, respectively. Moreover, in the error bars of Fig. 5(b), the maximum standard deviation is 3.52. The maximum FWHM in the experiment is 162 nm. The standard deviation of the spectral variation calculated by Eq. (5) is 1.124.

The refractive index sensing test was performed on the NCF coated with Ag/PDMS film. The temperature of the temperature-control box is adjusted to 25 °C. The refractive index of the solution to be tested ranges from 1.333 to 1.373.

Figure 6 reveals the transmission spectra at different refractive indexes. We can see that the resonant dips do not move as the refractive index changes.

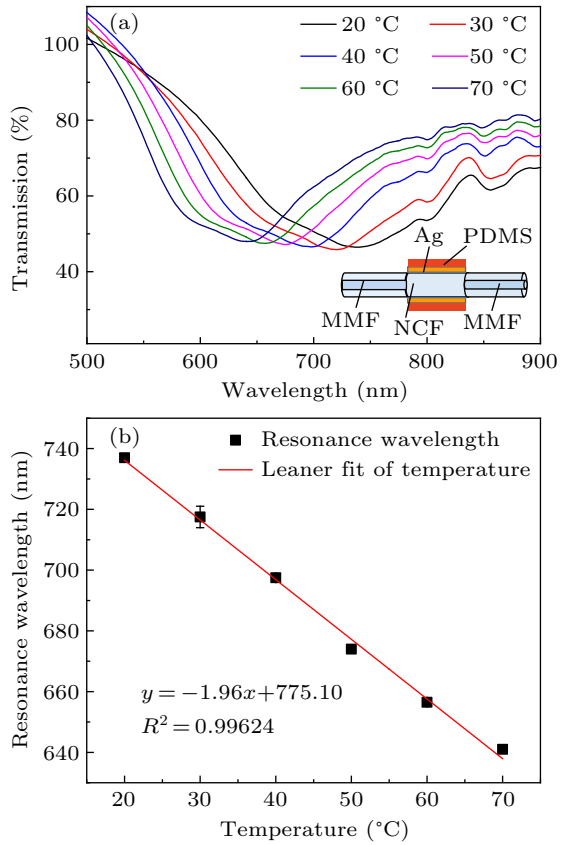


Fig. 5. (a) Transmission spectra at different temperatures, and (b) resonance wavelength variation with temperature.

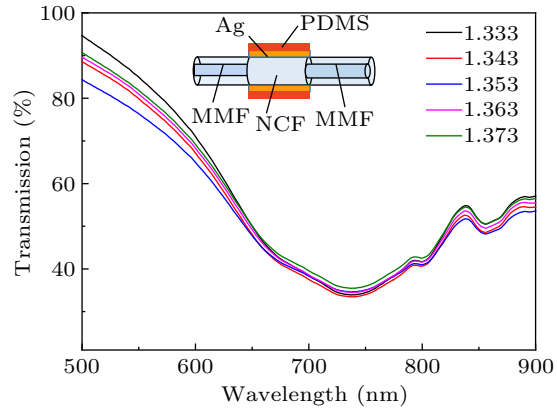


Fig. 6. Transmission spectra at different RI.

From this experiment, we can conclude that temperature has a greater influence on the sensor structure of NCF coated with Ag/PDMS film. The resonance drop appears near the wavelength range of 600 nm–800 nm. Since the PDMS film completely covers the NCF of the Ag-plated film, the solution and the Ag film are not in direct contact. The surface plasmon polaron (SPP) mode is not affected by changes in the refractive index of the liquid analyte. Therefore, changing the refractive index of the liquid to be measured will not cause a change in the resonance wavelength.

In this study, it is hoped that the sensor coated with PDMS film on the part of the sensing area of the Ag-coated NCF can achieve the effect of simultaneous measurements of refractive index and temperature. Therefore, it is necessary to have two resonance dips in a certain wavelength range: one is the refractive index sensing dip, and the other is the temperature sensing dip. From experiments 1 and 2, we know that the refractive index has a great influence on the structure of the NCF sensor with Ag film; meanwhile, the temperature has a great influence on the structure of the NCF sensor with Ag/PDMS film. We combined the two structures to conduct experiments for simultaneous measurements of refractive index and temperature.

We choose 2.8 cm Ag-coated NCF. The magnetron sputtering Ag-coating parameters are the same as the above experiment. We splice both ends of it with MMF. PDMS is coated on Ag-coated NCF, and the length covered by PDMS is half of the total length. We use a temperature-control box to keep the external temperature unchanged, and we change the analyte dropped on the sensor surface to measure the refractive index at first. Then, deionized water is added to the surface of the sensor to keep the refractive index unchanged, and the temperature is measured by adjusting the temperature-control box. When the outside temperature is 25 °C, deionized water with a refractive index of 1.33 is dropped on the surface of the optical fiber. As shown in Fig. 7, there are two resonance dips. The first dip was in the range of 500 nm–600 nm, and the second dip appears in the 600 nm–800 nm range. According to experiments 1 and 2, it can be concluded that the two dips are respectively caused by the part of the NCF coated with the Ag film and the part of NCF with Ag-PDMS film.

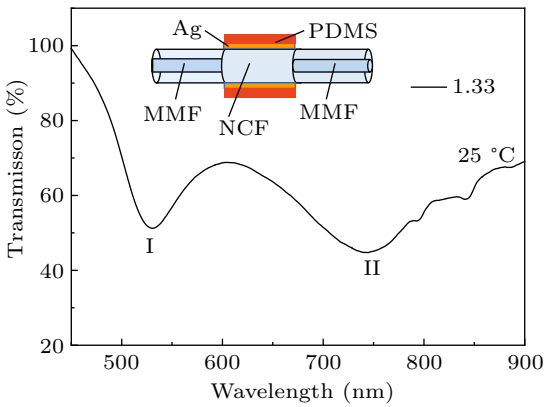


Fig. 7. Transmission spectra at a liquid analyte RI of 1.33 and temperature of 25 °C.

During the measurement of the refractive index, the outside temperature is controlled at 25 °C. The analyte added to the fiber's surface is changed to measure the refractive index. The refractive index range is 1.333 to 1.363. The transmission spectrum at the refractive index from 1.333 to 1.363 is shown in Fig. 8(a). It can be seen that as the RI of the liquid increases, dip I has a red shift and dip II has not changed. Figure 8(b)

shows the fit of the refractive index to the wavelength of its resonance dips. The linear fitting expression of the resonant wavelength of dip I with the RI is $y = 2121.43x - 1196.54$, where y and x represent the resonance wavelength and RI, respectively. The sensitivity of the RI in dip I and the linearity R^2 of dip I are 2121.43 nm/RIU and 0.99752, respectively. The sensitivity of the RI in dip II is 0 nm/RIU. This is consistent with experiment 2.

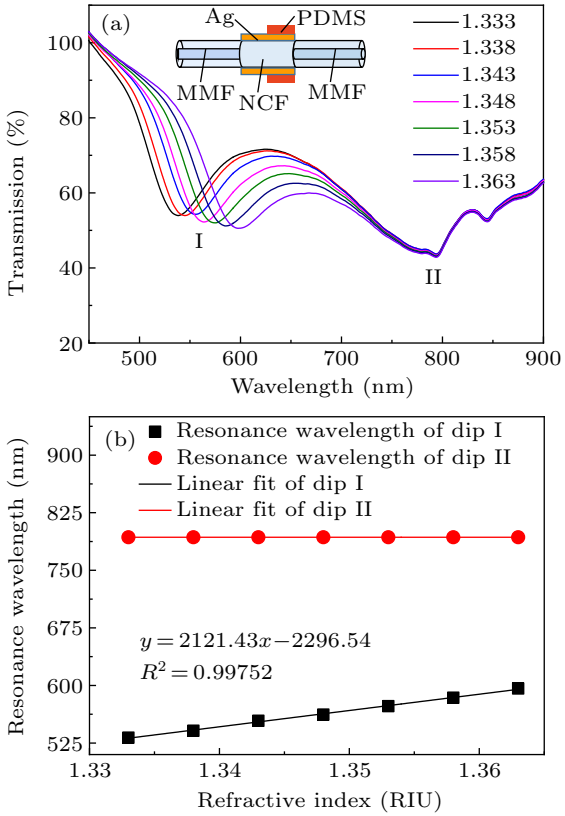


Fig. 8. (a) Transmission spectra at different RI, and (b) resonance wavelength variation with RI.

The external refractive index is controlled at 1.33, and the temperature-control box is adjusted for temperature measurement. The temperature range is 35 °C–60 °C. Figure 9(a) shows the transmission spectrum from low to high temperature. As the temperature increases, dip I and dip II both produce a blue shift. The fitting of temperature and its resonance dip's wavelength is shown in Fig. 9(b). The linear fitting expression of the resonant wavelength of dip I with temperature is $y = -0.32x + 542.97$, and the linear fitting expression of dip II with temperature is $y = -2.21x + 831.64$, where y and x represent the resonance wavelength and temperature, respectively. The temperature sensitivity in dip I and the linearity R^2 of dip I are -0.32 nm/°C and 0.9714, respectively. The temperature sensitivity in dip II is -2.21 nm/°C and the R^2 is 0.98922. The temperature sensitivity of dip I is lower, which is in line with experiment 1.

The matrix expression of temperature and refractive index can be deduced below based on

$$\begin{bmatrix} \Delta T \\ \Delta n \end{bmatrix} = K^{-1} \cdot \begin{bmatrix} \Delta\lambda_{\mathrm{I}} \\ \Delta\lambda_{\mathrm{II}} \end{bmatrix} = \begin{bmatrix} K_{T\mathrm{I}} & K_{n\mathrm{I}} \\ K_{T\mathrm{II}} & K_{n\mathrm{II}} \end{bmatrix}^{-1} \cdot \begin{bmatrix} \Delta\lambda_{\mathrm{I}} \\ \Delta\lambda_{\mathrm{II}} \end{bmatrix}. \quad (6)$$

By substituting the four coefficients $K_{T\mathrm{I}}$, $K_{T\mathrm{II}}$, $K_{n\mathrm{I}}$, and $K_{n\mathrm{II}}$ into formula (6), and $K_{T\mathrm{I}} = -0.3$ nm/°C, $K_{T\mathrm{II}} = -1.06$ nm/°C, $K_{n\mathrm{I}} = 1371$ nm/RIU, and $K_{n\mathrm{II}} = 1228$ nm/RIU, we can obtain the matrix expression of temperature and the refractive index

$$\begin{bmatrix} \Delta T \\ \Delta n \end{bmatrix} = \begin{bmatrix} -0.32\ \mathrm{nm/°C} & 2121.43\ \mathrm{nm/RIU} \\ -2.21\ \mathrm{nm/°C} & 0\ \mathrm{nm/RIU} \end{bmatrix}^{-1} \cdot \begin{bmatrix} \Delta\lambda_{\mathrm{I}} \\ \Delta\lambda_{\mathrm{II}} \end{bmatrix}. \quad (7)$$

According to Eq. (7), the temperature and refractive index can be determined by monitoring the two resonance wavelengths of dip I and dip II.

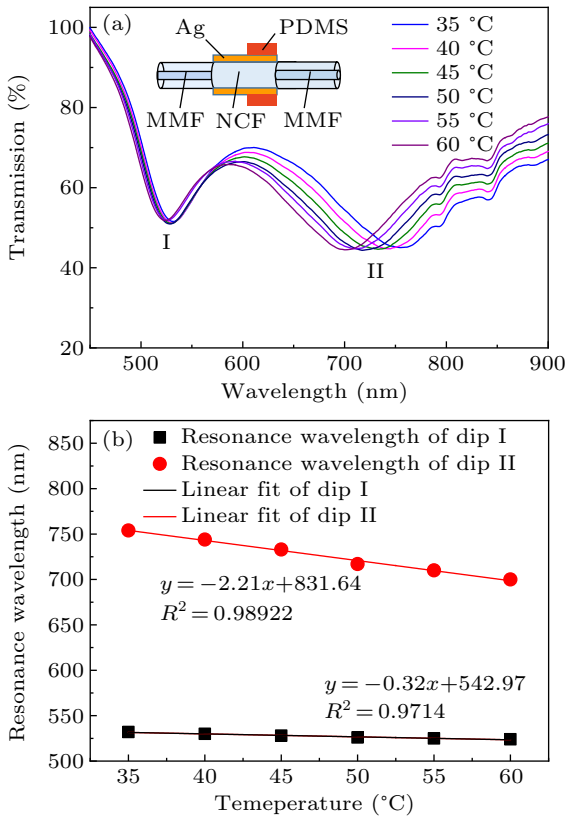


Fig. 9. (a) Transmission spectra at different temperatures, and (b) resonance wavelength variation with temperature.

To verify the hysteresis of the designed sensor, we control the temperature at 25 °C, and measure the refractive index increasing from 1.333 to 1.363 and decreasing from 1.363 to 1.333. Figure 10(a) shows the wavelength corresponding to each dip. It can be seen that the resonant wavelength obtained from the high to low refractive index almost coincides with the resonant wavelength obtained from the low to high refractive index. We also controlled the refractive index of 1.33, and performed warming and cooling experiments. Figure 10(b) shows wavelengths corresponding to each dip when warming and cooling. It can be seen that the resonance wavelength obtained from the heating experiment is almost consistent with

the resonance wavelength obtained from the cooling experiment. The resonant wavelength shifts obtained by the positive and negative experiments of the prepared sensor are consistent, which indicates that the prepared optical fiber SPR sensor has good test accuracy.

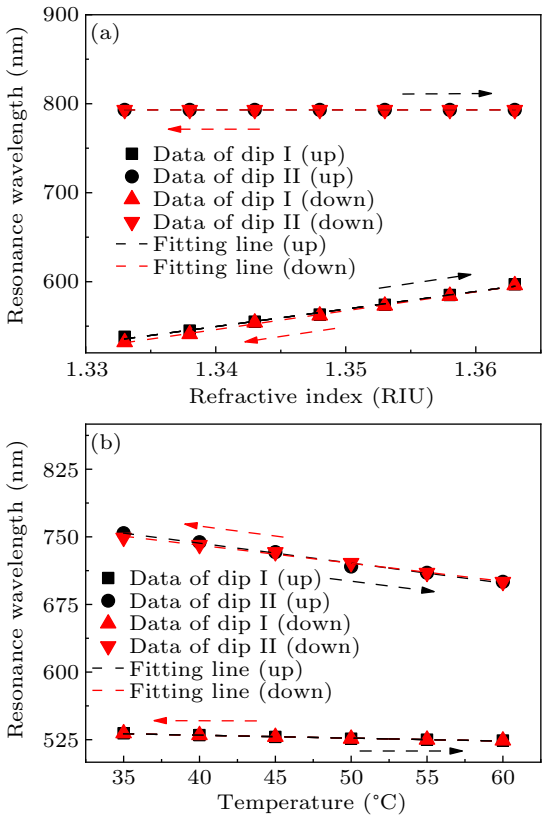


Fig. 10. (a) Resonance wavelength variation with RI, and (b) resonance wavelength variation with temperature.

3. Conclusion

In this work, we experimentally proved an SPR-based NCF sensor, which enabled the simultaneous measurements of RI and temperature. One part of the NCF in this sensor was coated with Ag/PDMS multilayer films to sense the ambient temperature, while the other part was just coated with a Ag film to sense the change in RI and temperature. The experimental results showed that the refractive index sensitivity and R^2 for dip I were 2121.43 nm/RIU and 0.99752, respectively, while the refractive index sensitivity was 0 nm/RIU for dip II. The temperature sensitivity and R^2 for peak I were -0.32 nm/°C and 0.9714, while they were -2.21 nm/°C and 0.98922 for dip II, respectively. By monitoring the wavelength shifts of the two dips, the refractive index and temperature could be demodulated and measured simultaneously with the transmission matrix method. This sensor structure has an important reference value for multi-parameter sensing.

Acknowledgments

Project supported by the Natural Science Foundation of Hebei Province, China (Grant No. F2021203112), the National Natural Science Foundation of China (Grant No. 12074331), the National Key Research and Development Program of China (Grant No. 2019YFB2204001), and Basic Scientific Research Funds for universities in Hebei Province, China (Grant No. JQN2021019).

References

[1] Chen H L, Li S G, Li J S and Fan Z K 2015 *IEEE Photon. Technol. Lett.* **27** 717
[2] Liu Y C, Chen H L, Li S G, Liu Q and Li J S 2017 *Chin. Phys. B* **26** 104211
[3] Wong W R, Krupin O, Sekaran S D, Adikan F R M and Berini P 2014 *Anal. Chem.* **86** 1735
[4] Bai Y T, Miao Y P, Zhang H M and Yao J Q 2020 *J. Light. Technol.* **38** 840
[5] Wang M H, Chen H L, Jing X L, Li S G, Ma M J, Zhang W X and Zhang Y Y 2020 *Optik* **219** 165044
[6] Momota M R and Hasan M R 2018 *Opt. Mater.* **76** 287
[7] Homola J 2003 *Anal. Bioanal. Chem.* **377** 528
[8] Wu L, Chu H S, Koh W S and Li E P 2010 *Opt. Express* **18** 14395
[9] Liu Z H, Liu L, Zhu Z D, Zhang Y, Wei Y, Zhang Y X, Yang J and Yuan L B 2017 *Opt. Commun.* **403** 290
[10] Chen H L, Li S G, An G W, Li J S, Fan Z K and Han Y 2015 *Plasmonics* **10** 57
[11] Chen H L, Li S G, Ma M J, Fan Z K and Wu Y D 2015 *Plasmonics* **10** 1239
[12] Chen Y and Ming H 2012 *Photonic Sens.* **2** 37
[13] Zhang Y Y, Chen H L, Wang M Y, Liu Y D, Fan X Y, Chen Q and Wu B 2021 *Mater. Res. Express* **8** 085201
[14] Yang X C, Lu Y, Liu B L and Yao J Q 2017 *Appl. Opt.* **56** 4369
[15] Wang B T and Wang Q 2018 *IEEE Sens. J.* **18** 8303
[16] Homola J 2008 *Chem. Rev.* **108** 462
[17] Voisin V, Caucheteur C, Mégret P and Albert J 2011 *Appl. Opt.* **50** 4257
[18] Zhang Y S, Li Y L, Wu Z Q, Hu S, Li Z B, Liu X Y, Yu J H, Huang Y M, Jing G Y, Lu H H, Guan H Y, Qiu W T, Dong J L, Zhu W G, Tang J Y, Luo Y H, Zhang J and Chen Z 2018 *Opt. Mater. Express* **8** 3927
[19] Zhang Y, Liu M J, Zhang Y X, Liu Z H, Yang X H, Zhang J Z, Yang J and Yuan L B 2020 *Appl. Opt.* **59** 1225
[20] Liu S H, Zhang H L, Li L T, Xiong L M and Shum P P 2019 *IEEE Photon. Technol. Lett.* **31** 189
[21] Sun L L, Qin J, Tong Z R, Zhang W H and Gong M J 2018 *Opt. Commun.* **426** 506
[22] Zhao Y, Wu Q L and Zhang Y N 2019 *Measurement* **148** 106792
[23] Caucheteur C, Guo T and Albert J 2015 *Anal. Bioanal. Chem.* **407** 3883
[24] Zhao Y, Deng Z Q and Wang Q 2014 *Sens. Actuator B Chem.* **192** 229
[25] Zhang Y N, Tao S Y E B R, Wu Y Q and Han B 2019 *IEEE Trans. Instrum. Meas.* **68** 4566
[26] Zhang Y Y, Chen H L, Wang M Y, Liu Y D, Fan X Y, Chen Q and Wu B 2021 *Mater. Res. Express* **8** 085201
[27] Zhao Y, Wu Q L and Zhang Y N 2018 *Sen. Actuator B-Chem.* **258** 822
[28] White I M Fan X 2008 *Opt. Express* **16** 1020
[29] Liu Y D, Chen H L, Li H Y, Zhang S, Gao Z G, Feng Y H, Zhang Y Y and Li S G 2021 *J. Opt. Soc. Am. B.* **38** 2536
[30] Wei Y, Wu P, Zhu Z D, Liu L, Liu C L, Hu J X, Wang S F and Zhang Y H 2018 *Sensors* **18** 3210